Loss of Tsc1 from striatal direct pathway neurons impairs endocannabinoid-LTD and enhances motor routine learning

Katelyn N. Benthall[1], Katherine R. Cording[2], Alexander H.C.W. Agopyan-Miu[1], Emily Y. Chen[1], and Helen S. Bateup[1,2,3*]

[1]Department of Molecular and Cell Biology, University of California, Berkeley, Berkeley, CA 94720, USA; [2]Helen Wills Neuroscience Institute, University of California, Berkeley, Berkeley, CA 94720, USA; [3]Chan Zuckerberg Biohub, San Francisco, CA 94158, USA.

*Correspondence:
Helen S. Bateup, Ph.D.
University of California, Berkeley
142 Life Sciences Addition
Berkeley, CA 94720 USA
Tel: (510) 664-4010
Email: bateup@berkeley.edu

Abstract

Tuberous Sclerosis Complex (TSC) is a neurodevelopmental disorder in which individuals frequently present with autism spectrum disorder (ASD). A core diagnostic criterion for ASD is the presence of restricted, repetitive behaviors (RRBs), which may result from abnormal activity in striatal circuits that mediate motor learning, action selection and habit formation. Striatal control over motor behavior relies on the coordinated activity of two subtypes of principle neurons, direct pathway and indirect pathway spiny projection neurons (dSPNs or iSPNs, respectively), which provide the main output of the striatum. To test if altered striatal activity is sufficient to cause repetitive behaviors in the context of TSC, we conditionally deleted *Tsc1* from dSPNs or iSPNs in mice and measured the consequences on synaptic function and motor behavior. We find that mice with loss of Tsc1 from dSPNs, but not iSPNs, have enhanced motor routine learning in the accelerating rotarod task. This increased motor learning is associated with an impairment in endocannabinoid-mediated long-term depression (eCB-LTD) at cortico-dSPN synapses in the dorsal striatum. Consistent with a loss of eCB-LTD, disruption of Tsc1 in dSPNs, but not iSPNs, results in a strong enhancement of corticostriatal synaptic drive. Together these findings demonstrate that within the striatum dSPNs show selective sensitivity to Tsc1 loss and indicate that enhanced activation of the striatal direct pathway is a potential contributor to RRBs in TSC.

Introduction

Autism spectrum disorder (ASD) is characterized by social and communication deficits, as well as the presence of restricted and repetitive behaviors (RRBs) [1]. A growing body of evidence suggests a strong genetic component to ASD as hundreds of genes have been associated with ASD risk [2-4]. These genes include those that cause syndromic disorders in which ASD is frequently diagnosed, together with a constellation of other neurological, psychiatric and medical conditions [5]. One such neurodevelopmental syndrome is Tuberous Sclerosis Complex (TSC), a disorder caused by mutations in either *TSC1* or *TSC2*, in which about half of patients meet the clinical criteria for an ASD diagnosis and most have epilepsy [6]. Under normal conditions, the TSC1 and TSC2 proteins form a heterodimer that negatively regulates the mTORC1 signaling pathway, a central signaling hub controlling cellular metabolic processes such as protein and lipid synthesis, cell growth, and autophagy [7]. In the case of loss of function of the TSC1/2 complex, the mTORC1 pathway is constitutively active, leading to excessive cell growth and altered cellular metabolism. Dysregulation of mTORC1 signaling is not limited to TSC but may occur commonly in ASD, with up to 15% of ASD cases directly attributable to altered mTORC1 signaling [8-10].

While epilepsy in TSC likely arises from altered excitability in forebrain circuits, the brain regions and cell types important for ASD-related behaviors in individuals with TSC are less well understood. We hypothesized that alterations in striatal circuits, which mediate motor learning, action selection and habit formation, might contribute to the RRBs observed in TSC patients with ASD [11]. Indeed, striatal dysfunction has been implicated in non-syndromic forms of ASD by structural and functional MRI studies [12-14]. Further, in a study of TSC children with and without ASD, striatal metabolism was found to be different specifically in those children with ASD [15]. Notably, this altered striatal activity was correlated with the presence of RRBs in the TSC children with ASD [15].

Mouse studies support these findings, showing that mutations in ASD-risk genes endow the striatum with an enhanced ability to acquire motor routines, a proposed explanation for the generation of RRBs [11, 16-19]. Functionally, changes in striatal synaptic properties have been reported in multiple ASD mouse models, suggesting that striatal alterations in ASD occur at the level of synapses [11, 17, 20-22]. Our group has previously shown input- and cell type-specific changes in synaptic transmission in striatal neurons with postnatal loss of Tsc1 [23]. Therefore, the goal of this study was to determine whether these synaptic changes are sufficient to cause RRBs.

Striatal function depends on the coordinated activity of two subpopulations of GABAergic projection neurons: direct pathway spiny projection neurons (dSPNs) and indirect pathway spiny projection neurons (iSPNs) [24]. These two subpopulations are anatomically intermingled in the striatum but are biochemically, morphologically, and physiologically distinct [25-27]. dSPNs preferentially express D1 dopamine receptors, while iSPNs express D2 dopamine receptors and A2a adenosine receptors. dSPNs and iSPNs are also distinct in their projection targets, diverging as they leave the striatum to innervate the globus pallidus internal segment (GPi) and substantia nigra pars reticulata (SNr), or the globus pallidus external segment (GPe), respectively [27]. At the simplest level, activation of dSPNs increases motor behaviors and action selection while stimulation of iSPNs inhibits movement [28, 29]. Therefore, coordinated activity between dSPNs and iSPNs allows for the selection of appropriate actions to be performed for any given context, while inappropriate actions are suppressed [30, 31]. Cortical and thalamic inputs make the primary glutamatergic synapses onto SPNs, and modification of the strength of this excitatory drive by long-term synaptic plasticity mediates motor learning and habit formation [32].

To determine how developmental loss of Tsc1 affects striatal synapses and whether this is sufficient to alter motor behaviors, we generated mice in which *Tsc1* was selectively deleted from either dSPNs or iSPNs. We find that motor routine learning is enhanced in mice with *Tsc1* deletion restricted to dorsal striatal dSPNs, but not iSPNs, which also occurs in mice with global haploinsufficiency of *Tsc2*. Further, we find that loss of Tsc1 causes a non-cell autonomous enhancement in corticostriatal drive of dSPNs but not iSPNs. Mechanistically, this is associated with a loss of retrograde endocannabinoid-mediated long-term depression (eCB-LTD) at corticostriatal synapses onto dSPNs. Together, these findings demonstrate that increased corticostriatal drive of dSPNs resulting from Tsc1/2 loss is sufficient to enhance the establishment of fixed motor routines.

Materials and Methods

Mouse lines

Animal experiments were performed in accordance with protocols approved by UC Berkeley's Animal Care and Use Committee. Male and female mice were used for all experiments. The ages used are indicated below for each experiment. All mice used for experiments were heterozygous or hemizygous for the *Ai9*, *Drd1-Cre*, *Adora2a-Cre*, or *Thy1-ChR2-YFP* transgenes to avoid potential physiological or behavioral alterations.

The following mouse lines were used:

Mouse line	Source	Reference
Tsc1$^{fl/fl}$	JAX strain #005680	[33]
Drd1a-Cre (EY217)	GENSAT (MMRRC #030778-UCD)	[34]
Adora2a-Cre (KG139)	GENSAT (MMRRC #031168-UCD)	[34]
Ai9 (tdTomato)	JAX strain #007909	[35]
Thy1-ChR2-YFP	JAX strain #007612	[36]
Tsc2$^{+/-}$	JAX strain #004686	[37]

Immunohistochemistry

Mice (P40-50) were perfused transcardially with 1x PBS and 4% paraformaldehyde. Brains were post-fixed in 4% paraformaldehyde overnight, cryoprotected in sucrose, and sectioned coronally at 30 µm. Sections were blocked for 1 hr at room temperature (RT) in BlockAid (Thermo Fisher Scientific) and incubated for 48 hr at 4°C with antibodies against phosphorylated S6 ribosomal protein (Ser240/244, 1:800, Cell Signaling Technology, catalog # 5364S), GFP (1:1000, Abcam, catalog # ab13970) and NeuN (1:800, Millipore, catalog # MAB377). Sections were washed and incubated for 1 h at RT with Alexa Fluor 633- and 488-conjugated secondary antibodies (1:500, Invitrogen, catalog #'s A-21070 and A-31553). Sections were mounted onto slides using Vectashield reagent with DAPI (Vector Labs).

Confocal imaging and analysis

To analyze p-S6 levels and soma volume, z-stack images of striatal sections were taken on a confocal microscope (Zeiss LSM 780 AxioExaminer) with a 20x objective using the same acquisition settings for each section. For quantification, cellular regions of interest (ROIs) were automatically created based on the tdTomato signal with the Surfaces module in Imaris software

(Oxford Instruments). The mean p-S6 fluorescence intensity per ROI and average soma volume were calculated using Imaris.

To analyze Cre-mediated recombination patterns in *Drd1*- and *Adora2a-Cre;Ai9* mice, z-stack images of dorsolateral striatum, dorsomedial striatum, nucleus accumbens lateral shell, and nucleus accumbens medial shell were taken on a confocal microscope (Olympus FLUOVIEW FV3000) with a 20x objective. For quantification, ROIs were manually defined in ImageJ for all NeuN positive cells and used to determine percent co-localization with the Cre-dependent tdTomato signal.

To analyze AAV-FLEX-TRAP (EGFP-L10a) expression, z-stack images of dorsal striatum were taken on a confocal microscope (Olympus FLUOVIEW FV3000) with a 20x objective. For quantification, ROIs were manually defined in ImageJ for all GFP positive cells and used to verify co-localization with the Cre-dependent tdTomato signal. 85-93% of EGFP-L10a positive cells in the dorsal striatum were tdTomato positive.

Dendritic spine imaging and analysis

Neonatal dSPN-Tsc1 KO mice were cryoanesthetized and injected bilaterally with 200 nL AAV9.CAG.Flex.tdTomato.WPRE.bGH (AllenInstitute864), diluted 1:500 to achieve sparse transduction. Injections were targeted to striatum, with coordinates approximately 1.2 mm lateral to midline, 2.0 mm posterior to bregma, and 1.5 mm ventral to the head surface. At age P40-50, mice were perfused and brains were post-fixed with 4% paraformaldehyde, then sectioned at 80 μm. Sections were blocked for 1 hr at RT in BlockAid (Thermo Fisher Scientific) and incubated for 48 hr at 4°C with antibody against RFP (1:1000, Rockland (VWR), catalog #RL600-401-379). Sections were washed and incubated for 1 h at RT with Alexa Fluor 546 secondary antibody (1:500, Invitrogen, catalog #A-11035). Sections were mounted onto slides using Vectashield reagent with DAPI (Vector Labs). Z-stack images of individual dendrites were taken on a confocal microscope (Zeiss LSM 880 NLO AxioExaminer) with a 63x objective using Airyscan super-resolution imaging. To quantify spine density, dendrites and spines were reconstructed using the FilamentTracer module in Imaris software (Oxford Instruments). The spine density of each dendrite was calculated using Imaris.

Behavioral analysis

Behavior studies were carried out in the dark phase of the light cycle under red lights (open field) or white lights (rotarod). Mice were habituated to the behavior testing room for at least 30 min prior to testing and covered by a black-out curtain. Mice were given at least one day between different tests. All behavior equipment was cleaned between each trial and mouse with 70% ethanol, and additionally rinsed in diluted soap followed by water at the end of the day. If male and female mice were to be tested on the same day, male mice were run in behavior first then returned to the husbandry room, after which all equipment was thoroughly cleaned prior to bringing in female mice for habituation. All animals to be tested from a given cage were run in each behavior test in the same day. Behavioral tests were performed with young adult male and female mice (6-10 weeks old). The experimenter was blind to genotype throughout the testing and scoring procedures.

Open field

Exploratory behavior in a novel environment and general locomotor activity were assessed by a 60 min session in an open field chamber (40 cm L x 40 cm W x 34 cm H) made of transparent plexiglass. Horizontal photobeams to measure rearing were positioned at 9 cm of height. The mouse was placed in the bottom right hand corner of the arena and behavior was recorded using an overhead camera and analyzed using the ANY-maze (Stoelting Co.) behavior tracking software. An observer manually scored self-grooming behavior during the first 20 minutes of the test.

Rotarod

The accelerating rotarod test was used to examine motor learning. Mice were tested on a rotarod apparatus (Ugo Basile: 47650) for 4 consecutive days. Three trials were completed per day with a 5 min break between trials. The rotarod was accelerated from 5-40 revolutions per minute (rpm) over 300 s for trials 1-6 (days 1 and 2), and from 10-80 rpm over 300 s for trials 7-12 (days 3 and 4). On the first testing day, mice were acclimated to the apparatus by being placed on the rotarod rotating at a constant 5 rpm for 60 s and returned to their home cage for 5 minutes prior to starting trial 1. Latency to fall, or to rotate off the top of the rotarod barrel, was measured by the rotarod stop-trigger timer.

Slice preparation for electrophysiology

Mice were perfused transcardially with ice-cold ACSF (pH=7.4) containing (in mM): 127 NaCl, 25 $NaHCO_3$, 1.25 NaH_2PO_4, 2.5 KCl, 1$MgCl_2$, 2 $CaCl_2$, and 25 glucose, bubbled continuously with carbogen (95% O_2 and 5% CO_2). Brains were rapidly removed and coronal slices (275 µm) were cut on a VT1000S vibrotome (Leica) in oxygenated ice-cold choline-based external solution (pH=7.8) containing (in mM): 110 choline chloride, 25 $NaHCO_3$, 1.25 $NaHPO_4$, 2.5 KCl, 7 $MgCl_2$, 0.5 $CaCl_2$, 25 glucose, 11.6 sodium ascorbate, and 3.1 sodium pyruvate. Slices were recovered in ACSF at 34°C for 15 minutes and then kept at RT before recording.

Whole-cell patch-clamp recording

Recordings were made with a MultiClamp 700B amplifier (Molecular Devices) at RT using 3-5 MOhm glass patch electrodes (Sutter, BF150-86-7.5). Data was acquired using ScanImage software, written and maintained by Dr. Bernardo Sabatini (https://github.com/bernardosabatini/SabalabAcq). Traces were analyzed in Igor Pro (Wavemetrics). Recordings with a series resistance >25 MOhms or holding current above -200 pA were rejected.

Current-clamp

Current clamp recordings were made using a potassium-based internal solution (pH=7.4) containing (in mM): 135 $KMeSO_4$, 5 KCl, 5 HEPES, 4 Mg-ATP, 0.3 Na-GTP, 10 phosphocreatine, and 1 ETGA. For corticostriatal excitability experiments, optogenetic stimulation consisted of a full-field pulse of blue light (470 nm, 0.15 ms for iSPNs or 0.5 ms for dSPNs) through a 63x objective. No synaptic blockers were included. For intrinsic excitability experiments, NBQX (10 µM, Fisher, cat. #104410), CPP (10 µM, Fisher, cat. #24710) and picrotoxin (50 µM, Abcam, cat. #120315) were added to the external solution to block synaptic transmission. 500 ms depolarizing current steps were applied to induce action potentials. No holding current was applied to the membrane.

Voltage-clamp

Voltage-clamp recordings were made using a cesium-based internal solution (pH=7.4) containing (in mM): 120 $CsMeSO_4$, 15 CsCl, 10 TEA-Cl, 8 NaCl, 10 HEPES, 1 EGTA, 5 QX-314, 4 Mg-ATP, and 0.3 Na-GTP. Recordings were acquired with the amplifier Bessel filter set at 3 kHz. Miniature excitatory synaptic currents (mEPSCs) were recorded in the presence of TTX (1 µM, Abcam, cat. #120055) to prevent action potential-mediated release. Picrotoxin (50 µM, Abcam, cat. #120315) and CPP (10 µM, Fisher, cat. #24710) were included for mEPSC

experiments to isolate AMPAR-mediated events. Corticostriatal synaptic stimulation experiments to measure evoked AMPA-mediated EPSCs were performed in picrotoxin (50 μM) and CPP (10 μM), and optogenetic stimulation consisted of a full-field pulse of blue light (470 nm, 0.15 ms) through a 63x objective. To measure AMPA/NMDA ratio, experiments were performed in 50 μM picrotoxin and the membrane was held at different potentials to isolate primarily AMPAR (-80 mV) or compound AMPAR and NMDAR (+40 mV) currents. The current at +40 mV was measured 50 ms after stimulation, by which time the AMPAR-mediated current has fully decayed.

DHPG-LTD

Endocannabinoid-mediated long-term depression (eCB-LTD) was induced in *Thy1-ChR2;Drd1-Cre;Ai9;Tsc1* mice by bath application of the group 1 mGluR agonist DHPG (100 μM, Sigma, cat. #D3689) for 10 min, following a 10 min baseline measurement of EPSC amplitude with single full field light pulses (3-15% light intensity, 0.15 ms) delivered every 30 seconds to stimulate corticostriatal terminals. Light intensity was adjusted for each cell to evoke 500-700pA currents during the baseline period. DHPG was subsequently washed off and EPSC amplitude was monitored every 30 sec for an additional 40 min. Picrotoxin (50 μM) was added to the bath during eCB-LTD experiments to isolate excitatory events, and perfusion flow rate was set to 5 mL/min. Cells were held at -50 mV to facilitate opening of L-type calcium channels. CB1R antagonist AM-251 (10 μM, Fisher, cat. #111710) was added to the bath during a subset of eCB-LTD experiments with dSPN-Tsc1 WT cells to verify that the LTD observed during these experiments was dependent upon CB1R activation. For CB1R agonism experiments, WIN2 (2 μM, EMD Millipore, cat. #5.04344.0001) was applied to the bath throughout the recording.

<u>AAV-Flex-TRAP plasmid and virus construction</u>

The AAV-hSyn-DIO-EGFP-L10a-WPRE-hGH and AAV-Ef1a-DIO-EGFP-L10a-WPRE-hGH plasmids were assembled from pAAV-hSyn-DIO-mCherry (Addgene plasmid #50459) and pAAV-EF1A-DIO-mCherry (Addgene plasmid #50462), which were gifts from Bryan Roth, and an EGFP-L10a construct, which was a gift from Anne Schaefer. AAV5 viruses were prepared by the University of Pennsylvania Vector Core with a titer of 5.97×10^{12} for AAV5-hSyn-DIO-EGFP-L10a-WPRE-hGH and 3.22×10^{12} for AAV5-Ef1a-DIO-EGFP-L10a-WPRE-hGH. The plasmids encoding these constructs and corresponding maps will be deposited on Addgene.

Intracranial virus injection

Mice were anesthetized with isoflurane and mounted on a stereotaxic frame equipped with ear cups. 800 nl of an AAV serotype 5 *Ef1a* or *hSyn* promoter-driven DIO-EGFP-L10a virus (AAV-FLEX-TRAP) was bilaterally injected into the dorsal striatum of 3-8 week old *Tsc1^{cKO};Drd1a-Cre(EY217)* mice. Coordinates for injection were +/-1.6 M/L, +0.6 A/P, -1.3 D/V. Mice were used for experiments 11-14 days after AAV-FLEX-TRAP virus injection.

Translating ribosome affinity purification (TRAP)

Anti-GFP magnetic bead preparation

Each TRAP experiment was performed on 6 samples in parallel, with dSPN-Tsc1-WT and Tsc1-KO mice processed together. For 6 mice, two batches of beads were prepped in parallel in separate tubes. TRAP was performed according to published methods [26, 38]. All steps were performed on ice unless otherwise noted. 450 µL of Dynabeads MyOne Streptavidin T1 (Lifetech cat #65601) were washed using a magnetic tube rack in RNase-free PBS and then incubated in Protein L solution (850 µL PBS + 150 µg Protein L) for 35 min at room temperature (RT). Beads were washed 5x with 3% IgG Protease-free BSA to block, then incubated with 150 µg of two different anti-GFP antibodies (19C8 and 19F7, Memorial Sloan Kettering Antibody and Bioresource Core), diluted in 900 µL PBS, for 1 hr at RT. Beads were then washed 3x in 0.15 M KCl buffer without cyclohexamide (-CHX), then resuspended in 630 µL of 0.15 M KCl (+CHX).

Brain lysate preparation and immunoprecipitation

Mice were anesthetized, and brains were dissected and blocked to contain mainly striatum. Bilateral striata from each animal were placed into glass homogenization tubes on ice, and pestles were inserted. Homogenization took place at 4°C (3 strokes at 300 RPM, 12 strokes at 900 RPM, Yamato Lab Stirrer LT400), care was taken to avoid generating bubbles. Lysates were poured into pre-chilled Eppendorf tubes and centrifuged for 10 min at 2,000 x g at 4 °C to precipitate large organelles. Samples were then transferred to a new pre-chilled tube and volumes were measured. 10% NP-40 (1/9 sample volume, ~70-80 µL) was added, then DHPC (1/9 new sample volume) was added, and samples were incubated on ice for 5 mins. DHPC stock is 200 mg dissolved in 1.38 mL ddH2O. Samples were then centrifuged for 10 min at 16,000 x g at 4 °C to precipitate mitochondria. Antibody-bound beads were resuspended by inversion, and 200 µL of beads were added to 6 separate tubes. Supernatants from samples were then transferred into tubes with beads and incubated on rotators at 4 °C overnight.

Isolation and purification of RNA

Samples were spun down briefly and placed on magnets pre-chilled on ice. Supernatants were collected and transferred to pre-chilled "unbound" tubes. Beads were washed 4x with 0.35 M KCl buffer, with samples sitting on ice for 1 min between washes to reduce background binding. Beads were resuspended in 350 µL RLT-beta-ME. 100 µL of unbound samples were added separately to 350 µL RLT-beta-ME. Samples (bound and unbound) were then rotated for 10 min at RT. Samples were placed on the magnet and supernatants were removed and added into fresh tubes containing 350 µL of 80% EtOH, mixed, and then all 700 µL of sample + EtOH was added to RNeasy column (pre-chilled). 350 µL of unbound sample was also mixed with 350 µL of EtOH and added to RNeasy column. At this point there were 12 columns, one bound and one unbound sample for each mouse. Samples were centrifuged for 30 sec at 8000 x g at RT. Flow-through was passed through column twice more to repeat binding. Flow-through was then discarded and 500 µL of RPE buffer was added to each column and spun for 30 sec at 8000 x g. Flow-through was discarded and 500 µL of 80% EtOH was added to the column, spun for 2 min at 8000 x g at RT. Flow-through was discarded, and columns were dried by spinning for 5 mins at full speed with cap open. Dried columns were placed into new collection tubes (not pre-chilled) and 28 µL RNase-free water was added directly to the column membrane. Columns were incubated for 5 min at RT with caps closed, then spun for 1 min at max speed at RT. RNA concentration and quality was determined by NanoDrop and Bioanalyzer at the UC Berkeley Functional Genomics Laboratory core facility.

Quantitative PCR

Reverse transcription was performed using random hexamer primers and Superscript III reverse transcriptase (Lifetech, 18080051). Real-time PCR was performed in triplicate with 1 uL cDNA using a Biorad CFX384 thermal cycler with TaqMan Universal PCR Master Mix, no AmpErase UNG (Lifetech, 4324018) and TaqMan probes. The following TaqMan probes were used: *Grm1* (Mm01187086_m1), *Grm5* (Mm00690332_m1), *Homer1* (Mm00516275), *Plcb1* (Mm00479998), *Drd1* (Mm01353211_m1), *Drd2* (Mm00438545_m1), and *Actb* (Mm02619580_g1). Values for all mRNAs were normalized to *Actb* for each sample.

Statistical analyses

Two-tailed paired or unpaired two-tailed t-tests were used for comparisons between two groups, and an F-test was used to confirm that variances were not significantly different. For data that did not pass D'Agostino & Pearson normality test, Mann Whitney test was used. A one-way

ANOVA with Holm-Sidak's post-hoc tests was used to compare the means of three or more groups. For data that did not pass the D'Agostino and Pearson normality test, the Kruskal-Wallis test with Dunn's post-hoc tests was used. A two-way ANOVA or mixed effects analysis was used to compare differences between groups for experiments with two independent variables. P-values were corrected for multiple comparisons.

Results

Upregulation of mTORC1 and somatic hypertrophy in SPNs with Tsc1 deletion

To test whether striatal-specific disruption of the Tsc1/2 complex is sufficient to drive RRBs, we bred conditional *Tsc1* mice (*Tsc1*^{cKO}) with striatal-restricted *Drd1-Cre* or *Adora2a-Cre* mice [33, 34] to achieve dSPN- or iSPN-specific loss of Tsc1, respectively (Fig. 1a,b). In addition, we bred in a Cre-dependent tdTomato fluorescent reporter (*Ai9*) to visualize Cre-expressing cells [35]. We used the EY217 *Drd1-Cre* founder line from GENSAT as it has more striatal-restricted expression than the commonly used EY262 line (Fig. S1a,b). In preliminary studies, we found that *Tsc1*^{cKO}*;Drd1-Cre*(EY262) mice died prematurely, around post-natal day 15, which was not the case for Cre-positive *Tsc1*^{WT} or *Tsc1*^{cHet} animals. The premature mortality was likely driven by seizures due to cortical Cre expression in this line (Fig. S1b) as loss of Tsc1 from only a small percent of cortical neurons is sufficient to induce seizures [39]. *Tsc1*^{cKO}*;Drd1-Cre*(EY217) did not exhibit premature mortality, likely due to the more striatal-restricted Cre expression. Notably, Cre expression in *Drd1-Cre*(EY217) mice is highest in the dorsal striatum, with 40-50% of neurons showing Cre-dependent recombination, whereas less than 8% of neurons in the ventral striatum exhibit Cre activity (Fig. S1c-f, j). *Adora2a-Cre* is expressed uniformly throughout the striatum in approximately 45% of neurons (Fig. S1g-j, l).

To confirm that *Tsc1* deletion upregulated mTORC1 signaling in dSPNs and iSPNs, we quantified the phosphorylation of mTORC1 pathway target ribosomal protein S6 in dorsal striatal neurons from *Tsc1*^{cKO}*;Drd1-Cre;Ai9* (referred to as dSPN-Tsc1 KO) and *Tsc1*^{cKO}*;Adora2a-Cre;Ai9* (referred to as iSPN-Tsc1 KO) mice. Loss of Tsc1 caused a gene dose-sensitive increase in p-S6 levels in both dSPNs and iSPNs, indicating mTORC1 pathway hyperactivity in both cell types (Fig. 1c-f and h-k). Moderate somatic hypertrophy was also observed in dSPN-Tsc1 KO and iSPN-Tsc1 KO cells, consistent with the known role of mTORC1 signaling in regulating cell size (Fig. 1g,l). However, striatal neurons with heterozygous (Het) deletion of *Tsc1* did not exhibit increased soma size (Fig. 1g,l).

Loss of Tsc1 from dSPNs but not iSPNs enhances motor routine learning

To determine whether SPN-specific loss of Tsc1 was sufficient to alter motor behaviors relevant for ASD, we investigated general locomotor activity and self-grooming behavior in the open field. We found no significant differences in the total distance traveled, number of rears, or grooming bouts in dSPN- or iSPN-Tsc1 Het or KO mice compared to controls (Fig. 2a-f). These results suggest that loss of Tsc1 from a single SPN subtype is not sufficient to alter gross motor behavior or induce spontaneous stereotypies.

The accelerating rotarod task is a striatal-dependent motor learning assay [40] that is altered in multiple mouse models of ASD [16-19]. In this test, mice learn to run on a rod revolving at increasing speed over four days of training with three trials performed each day (Fig. S2a). Over the course of training, mice develop a stereotyped motor routine to stay on the apparatus for increasing amounts of time. Control mice improve at the task over training, with an average learning rate of 2-3 rpm/day. We found that dSPN-Tsc1 KO mice had similar initial rotarod performance on trial 1, reflecting normal baseline motor coordination (Fig. 2g; dSPN-Tsc1-WT mean=19.22 rpm, dSPN-Tsc1-Het mean=19.14 rpm, dSPN-Tsc1-KO mean=20.22 rpm; p=0.9996 (WT vs Het), p=0.9383 (WT vs KO), unpaired t-tests). However, dSPN-Tsc1 KO mice exhibited significantly enhanced motor learning measured as the slope of performance from the first to last trial for each mouse, compared to littermate controls (Fig. 2g,h). Interestingly, dSPN-Tsc1 Het animals displayed a mild enhancement of motor learning consistent with a gene dose-dependent effect (Fig. 2g). Strikingly, we found no change in either initial motor performance or motor learning ability in mice with iSPN-specific loss of Tsc1 (Fig. 2i,j.

Individuals with TSC usually have a germline heterozygous mutation in either *TSC1* or *TSC2*; however, “second-hit” somatic mutations causing loss of heterozygosity are thought to contribute to the cortical tubers that are a pathological hallmark of the disorder [41]. Additionally, “microtubers” and dysplastic cellular regions in subcortical structures, including the basal ganglia, have been identified in post-mortem TSC brains and proposed to contribute to ASD and cognitive disability in TSC [41]. That said, patients with little to no tuber burden can also be strongly impacted [42]. This has led to the idea that haploinsufficiency may contribute to brain phenotypes in TSC, in particular the behavioral and psychiatric aspects [8, 43]. To determine whether motor learning is altered by partial loss of function of Tsc1/2, we tested mice with a heterozygous germline *Tsc2* mutation in the accelerating rotarod. Similar to dSPN-Tsc1 KO mice, *Tsc2* Het mice had normal initial motor performance but exhibited a significant increase in motor learning compared to WT littermates that became apparent in the more challenging trials of the test (Fig. S2b,c). These results demonstrate that 1) haploinsufficiency of *Tsc1*/2 is sufficient to alter striatal-dependent motor learning and 2) disruption of *Tsc1* in dSPNs alone can promote the development of fixed motor routines.

Loss of Tsc1 increases cortical drive of direct pathway striatal neurons

Motor learning relies on corticostriatal transmission, therefore, changes in SPN response to cortical activity could account for enhanced motor routine acquisition in dSPN-Tsc1 KO mice.

Previous work identified increased cortico-dSPN but not thalamo-dSPN excitability in mice with postnatal *Tsc1* deletion [23]. However, whether this is also the case for mice with developmental disruption of *Tsc1* was unexplored. To test this, we crossed the *Tsc1*^{cKO}*;Drd1-Cre;Ai9* and *Tsc1*^{cKO}*;Adora2a-Cre;Ai9* mice to the *Thy1-ChR2-YFP* mouse line, which expresses channelrhodopsin (ChR2-YFP) in a subset of cortical layer V pyramidal cells (Fig. 3a) [36]. To simulate a train of cortical inputs, we applied ten light pulses over the recording site in dorsolateral striatum and recorded responses in SPNs in current-clamp mode in the absence of any blockers (Fig. 3b). By varying the intensity of cortical stimulation, either subthreshold depolarizations or action potentials (APs) could be elicited in SPNs with a given probability. We quantified the number of APs evoked by this stimulation paradigm as a percent of total stimulation events. The pulse train was repeated at different light intensities to generate an input-output curve of corticostriatal transmission. We found that cortical terminal stimulation significantly increased spike probability across all light intensities in dSPN-Tsc1 KO cells compared to WT (Fig. 3c,d). Notably, loss of one copy of *Tsc1* in dSPNs was sufficient to increase corticostriatal drive (Fig. 3c,d).

We performed the 10 pulse cortical stimulation experiment in iSPNs and found that WT iSPNs were more readily driven to spike than dSPNs, consistent with their increased intrinsic excitability [23, 25]. Therefore, we reduced the length of the light pulse to avoid saturating the response. Interestingly, the number of APs elicited from iSPNs during cortical stimulation was not different between genotypes at any light intensity (Fig. 3e,f). These results are highly consistent with the behavioral findings in the rotarod test and demonstrate that deletion of *Tsc1* has a selective impact on dSPNs, while iSPNs are remarkably unaffected.

Increased cortico-dSPN excitability results from enhanced synaptic transmission

Enhanced responses in dSPN-Tsc1 KO and Het mice to cortical terminal stimulation could result from increased intrinsic membrane excitability, increased synaptic excitation, or both. Indeed, *Tsc1* deletion has diverse effects on intrinsic and synaptic excitability depending on the cell type studied [23, 44-55]. To test if changes to intrinsic excitability occur in dSPN-Tsc1 KO neurons, we injected positive current and measured the number of APs fired as a function of current step amplitude. The input-output curve for dSPN-Tsc1 KO cells was shifted slightly to the right relative to dSPN-Tsc1 WT and Het neurons, indicating a small intrinsic membrane hypoexcitability (Fig. 3g,h).

Intrinsic hypoexcitability has been observed in other TSC mouse models [44, 46, 48, 52, 53], and may result from somatic hypertrophy (see Fig. 1). However, this does not explain the

enhanced corticostriatal excitability observed in dSPNs. To measure synaptic excitability, we recorded AMPA receptor (AMPAR)-mediated excitatory currents evoked by optical stimulation of cortical terminals (EPSCs) in *Tsc1^{cKO};Drd1-Cre;Ai9;Thy1-ChR2-YFP* mice. Stimulation of cortical terminals resulted in significantly larger AMPAR-mediated EPSCs in dSPN-Tsc1 KO and Het cells compared to WT cells, particularly at higher light intensities (Fig. 3l,j). When we measured the ratio of AMPAR currents recorded at -80 mV to NMDAR currents recorded at +40 mV, we found that AMPA:NMDA ratios were not significantly different across genotypes (Fig. 3k,l), suggesting a global enhancement of excitatory synaptic function rather than a selective change in receptor composition.

To investigate the specific synaptic properties that were altered in dSPN-Tsc1 KO and Het neurons, we recorded spontaneous miniature excitatory post-synaptic currents (mEPSCs) at six weeks of age and found increased amplitude and frequency of mEPSCs onto dSPN-Tsc1 KO cells compared to WT (Fig. 4a-c). An increase in mEPSC frequency but not amplitude was also observed in dSPN-Tsc1 Het cells (Fig. 4a-c). To determine the developmental timing of these changes, we recorded mEPSCs in dSPN-Tsc1 WT and KO neurons at 2, 3 and 4 weeks of age. We found that the increased mEPSC amplitude and frequency in dSPN-Tsc1 KO neurons compared to WT did not emerge until 4 weeks of age, a time when corticostriatal circuits are maturing and becoming refined [56] (Fig. S3a,b). Thus, loss of Tsc1 may not affect the initial development of excitatory synapses but could affect their activity-dependent refinement. Consistent with a lack of cortico-iSPN excitability change, no significant changes in mEPSC amplitude or frequency were observed in iSPN-Tsc1 KO or Het cells at 6 weeks of age (Fig. 4d-f).

While changes in mEPSC amplitude usually reflect increased post-synaptic AMPAR function, as observed in dSPN-Tsc1 KO and Het cells (see Fig. 3i,j), increased mEPSC frequency can result from more synaptic contacts or a change in presynaptic release probability. To measure synapse number, we labeled dSPNs in the dorsal striatum using an AAV expressing Cre-dependent tdTomato. In fixed striatal sections, we imaged and reconstructed individual dSPNs and quantified the density of dendritic spines, which are the sites of corticostriatal synapses onto SPNs [57]. We found that dSPN-Tsc1 KO neurons had equivalent spine density to dSPN-Tsc1 WT cells (Fig. 4g-k), suggesting that the increased mEPSC frequency was likely due to a change in presynaptic release probability.

Endocannabinoid-mediated long-term depression is impaired in dSPN-Tsc1 KO neurons

One mechanism that could explain enhanced presynaptic corticostriatal transmission onto dSPN-Tsc1 KO neurons is a loss of long-term synaptic depression (LTD), which would render cells unable to depress excitatory inputs. Corticostriatal terminals express CB1 receptors that mediate endocannabinoid-LTD (eCB-LTD), a prominent form of striatal synaptic depression [58, 59]. Upon coincident activation of group 1 metabotropic glutamate receptors (mGluR1/5) and L-type calcium channels, SPNs release the endocannabinoids anandamide (AEA) or 2-arachidonoylglycerol (2-AG), which act as retrograde signals that activate presynaptic CB1Rs to decrease corticostriatal release probability [58]. Historically it has been thought that eCB-LTD occurs in iSPNs and is absent in dSPNs [60], but recent studies using more selective stimulation of corticostriatal terminals have revealed eCB-LTD in both SPN subtypes [61]. Notably, since loss of another form of mGluR-dependent LTD expressed in the hippocampus is impaired in multiple TSC mouse models [45, 62-64], and selective disruption of 2-AG release from dSPNs causes enhanced excitation and repetitive behaviors [65], we reasoned that loss of eCB-LTD could occur in dSPNs with *Tsc1* deletion.

We induced eCB-LTD in dSPNs with wash-on of the group 1 mGluR agonist DHPG and monitored the amplitude of AMPAR-mediated events in response to optogenetic stimulation of cortical terminals in the dorsolateral striatum. While dSPN-Tsc1 WT neurons showed a long-lasting synaptic depression to ~79% of baseline levels, eCB-LTD did not occur in dSPN-Tsc1 KO neurons, which exhibited only a small initial reduction in EPSC amplitude during DHPG application that was not maintained (Fig. 5a). To ensure that the protocol was inducing eCB-LTD, we performed the DHPG wash-on in the presence of AM-251, a CB1R antagonist, and found that LTD was blocked in control dSPNs (Fig. S4). Further, these changes cannot be explained by a presynaptic difference in CB1R function, as direct activation of CB1Rs with the CB1R agonist WIN-2 depressed corticostriatal EPSCs to the same extent in *Tsc1* deleted and control dSPNs (Fig. 5b).

To investigate a potential molecular basis for the loss of eCB-LTD in Tsc1 KO dSPNs, we performed translating ribosome affinity purification (TRAP) to assess the translational status of mRNAs encoding key proteins in the eCB-LTD pathway in dSPNs. To do this, we engineered an AAV to express a Cre-dependent GFP-tagged ribosomal protein (EGFP-L10a) and injected this into the dorsal striatum of *Drd1-Cre;Ai9* mice that were WT or homozygous floxed for *Tsc1* (Fig. 5c,d). This approach enabled selective expression of EGFP-L10a in dSPNs (Fig. 5e). Using EGFP as an affinity tag, we isolated ribosome-bound mRNAs selectively from dSPNs using TRAP [26, 38]. We verified the specificity of this approach using qPCR to quantify the

relative levels of *Drd1* (D1R) and *Drd2* (D2R) mRNA in the TRAP samples compared to the unbound samples, which includes RNA from all striatal cell types. As expected, *Drd1* mRNA was significantly enriched in the TRAP samples from both dSPN-Tsc1 WT and dSPN-Tsc1 KO mice compared to the unbound samples (Fig. 5f). Accordingly, *Drd2* mRNA was depleted from the TRAP samples, demonstrating selective isolation of mRNA from dSPNs (Fig. 5g).

We compared the relative expression levels of mRNAs encoding proteins required for eCB-LTD including the two types of group 1 mGluRs (*Grm1* and *Grm5*), the requisite mGluR scaffold protein Homer 1 (*Homer1*), and phospholipase C beta (*Plcb1*), which promotes the formation of diacylglycerol that is subsequently converted to 2-AG by diacylglycerol lipase [58, 66]. We also compared the levels of ribosome-bound *Drd1* as a non-eCB-LTD control. We found that dSPN-Tsc1 KO mice had increased amounts of total ribosome-bound mRNA compared to WT (0.0518 +/- 0.0077 vs 0.0313 +/- 0.0031 ratio of TRAP-isolated mRNA to unbound RNA in dSPN KO vs WT mice, p=0.0138, unpaired t-test), consistent with a global increase in protein synthesis resulting from high mTORC1 activity. However, all four components of the eCB-LTD pathway showed a relative reduction in ribosome-bound mRNA levels in dSPN-Tsc1 KO mice compared to WT mice (Fig. 5h-k). Notably, levels of *Drd1* were not significantly different between genotypes (Fig. 5l). The amount of ribosome-bound mRNA is thought to reflect translation efficiency [67] (although some limitations must be considered, see [68]), therefore these results suggest a relative downregulation in the translation of multiple mRNAs encoding proteins required for eCB-LTD in Tsc1 KO dSPNs. Such decreased expression may be one mechanism responsible for the lack of functional eCB-LTD in Tsc1 KO dSPNs.

Discussion

In this study we tested whether cell type-specific deletion of *Tsc1* from striatal neurons was sufficient to induce repetitive motor behaviors related to ASD. We find that in both direct and indirect pathway SPNs, developmental loss of *Tsc1* upregulates mTORC1 signaling and increases soma size, consistent with other neuron types [23, 45-49]. However, we find that mTORC1 activation only in dSPNs, but not iSPNs, enhances motor routine learning in the absence of spontaneous stereotypies or locomotor hyperactivity. Further, we find that increased motor learning in dSPN-Tsc1 KO mice is associated with increased corticostriatal synaptic excitability and a loss of eCB-LTD. Notably, loss of only one copy of *Tsc1* is sufficient to increase cortical drive of dSPNs and enhance motor learning. These findings implicate the striatal direct pathway as a possible driver of repetitive behaviors in TSC and identify a potential synaptic mechanism contributing to this behavior.

It has been shown that loss of Tsc1 in either the cerebellum or thalamus is sufficient to cause social behavior deficits and spontaneous RRBs including repetitive self-grooming in TSC mouse models [46, 48]. Given the central role of the striatum in action selection and motor learning [32], we hypothesized that alterations in striatal circuits might also contribute to RRBs in the context of TSC. We found that dSPN or iSPN-specific *Tsc1* deletion was not sufficient to induce spontaneous repetitive behaviors, suggesting that other brain regions may be more important for executing these behaviors. Indeed, the striatum has been shown to be important for the proper sequencing of grooming action patterns but not the initiation of grooming bouts [69]. In line with this, a recent study demonstrated that striatal-specific loss of the ASD-risk gene *Shank3* was not sufficient to reproduce the repetitive self-grooming that is observed with global loss of *Shank3* but that this could be driven by loss of Shank3 from forebrain excitatory neurons [70].

Intriguingly, we found that mice with loss of Tsc1 in dorsal dSPNs had enhanced performance on the accelerating rotarod, a motor learning task that relies on SPN activity and corticostriatal transmission [40]. Previous work has shown that striatal mTORC1 signaling is critical for motor learning on the accelerating rotarod, as both pharmacological and genetic intrastriatal inhibition of mTOR signaling impairs rotarod learning [71]. Our results are congruent with these findings and show that the mTORC1-dependence of motor learning is bidirectional, as increasing mTORC1 activity in dSPNs enhances performance. Importantly, the accelerating rotarod task has recently been recognized as commonly affected in mice with mutations in ASD-risk genes, as at least 5 other ASD mouse models have enhanced rotarod performance [16-19, 72] (although this is not the case for all ASD-risk genes, see [22, 73]). Notably, an extended

accelerating rotarod task may be necessary to reveal motor learning phenotypes, as *Tsc1* and *Tsc2* heterozygous mice were reported to have no changes in rotarod performance when an abbreviated version of the task was used [74]. While most of the aforementioned ASD mouse models are global gene deletions in which brain regions and circuits outside of the striatum could contribute to the phenotype, two of these studies showed that disrupting ASD-risk genes (*Nlgn3* or *Chd8*) in dSPNs, but not iSPNs, was sufficient to increase rotarod learning. Interestingly, in these studies, ventral striatal disruption of the gene was responsible for the motor learning improvement. Here, deletion of *Tsc1* from SPNs was largely restricted to the dorsal striatum, and our findings are consistent with literature establishing the dorsal striatum's role in motor learning [40]. Further studies will be needed to explore the involvement of ventral striatal circuits in motor learning and elucidate the contribution of specific striatal sub-regions to motor phenotypes in TSC mouse models.

While enhanced motor routine learning may be a shared phenotype across multiple mouse models of ASD, the synaptic and cellular mechanisms driving this phenotype are likely to be distinct depending on the specific gene that is altered. In a prior study, dSPN-Nlgn3 KO mice displayed normal excitatory synaptic transmission and eCB-LTD, but had a deficit in synaptic inhibition [16]. In the global *Chd8*$^{+/-}$ model, there was increased spontaneous excitatory transmission onto SPNs; however, the SPN sub-type was not defined. Here we found that dSPN-Tsc1 KO and Het cells had strongly enhanced corticostriatal excitation that was due to increased synaptic, but not intrinsic, excitability. We have previously reported increased presynaptic release probability in dSPNs with postnatal loss of Tsc1 [23] and consistent with this, we found increased mEPSC frequency in the absence of changes to spine density in dSPN-Tsc1 KO neurons. Given that the cortical inputs were wild-type in our model, a potential explanation is a change in retrograde signaling from dSPNs to cortical terminals. Indeed, we found that eCB-LTD was absent in Tsc1 KO dSPNs despite normal presynaptic CB1 receptor function. This suggests that loss of Tsc1 and upregulation of mTORC1 signaling in dSPNs interferes with one or more post-synaptic processes required for this form of plasticity: 1) expression of group 1 mGluRs, 2) signaling downstream of mGluRs, and/or 3) synthesis and release of eCBs. In support of this idea, we found that multiple mRNAs encoding proteins required for eCB-LTD exhibited differential ribosome engagement in dSPN-Tsc1 KO cells compared to WT and were relatively reduced. Together, this suggests that loss of Tsc1 and deregulation of mTORC1 signaling in dSPNs impairs post-synaptic mGluR signaling via altered expression of key components of this pathway.

A chronic impairment of eCB-LTD in Tsc1 KO dSPNs could explain not only the increased mEPSC frequency but potentially the increased amplitude, as these synapses may have a greater capacity to undergo long-term potentiation, leading to increased AMPAR content and synaptic strengthening over time. In this way, the enhancement of excitatory transmission could be a developmental phenotype, such that early-life corticostriatal synaptic pruning doesn't properly occur due to loss of LTD [75], resulting in corticostriatal hyperactivity. This idea is consistent with our observation that changes in mEPSC properties in dSPN-Tsc1 KO neurons do not arise until four weeks of age and later, after the primary period of postnatal striatal maturation [76]. A causal role for impaired eCB-LTD in increased AMPAR function is also suggested by the finding that direct disruption of endocannabinoid synthesis and release from dSPNs is sufficient to increase their glutamatergic drive [65]. Interestingly, this prior study showed that disruption of 2-AG signaling in dSPNs had behavioral consequences while loss from iSPNs had no measurable effects on behavior [64], consistent with the lack of behavior changes reported here for iSPN-Tsc1 KO mice.

Taken together, our results support a model whereby developmental loss of Tsc1 from dSPNs impairs eCB-LTD resulting in unchecked corticostriatal drive. Such a change in presynaptic plasticity may alter corticostriatal coupling during rotarod training, leading to atypical learning in this paradigm. In terms of autistic behaviors in individuals with TSC, our findings suggest that striatal synaptic and circuit changes, which in animal models increase their ability to learn a stereotyped motor routine, could contribute to the emergence of restricted, repetitive patterns of behavior.

Acknowledgements

This work was supported by an NSF graduate research fellowship to K.N.B. (DGE 1106400), a SFARI Pilot Award (# 307866) to H.S.B., and R21 NS096415, R56 MH111821 and R01 NS105634 grants to H.S.B. H.S.B. is a Chan Zuckerberg Biohub Investigator and was supported by an Alfred P. Sloan Foundation fellowship. We thank Corinna Wong and Caroline Keeshen for their assistance with mouse colony maintenance. We thank John Blair for assistance with cloning the AAV-FLEX-TRAP construct. We thank Claire Darzacq for access to the qPCR equipment. We thank Anne Schaefer for advice on the TRAP protocol and for providing the EGFP-L10a construct. We thank Kamran Ahmed for generating the figure schematics. Confocal spine imaging experiments were conducted at the CRL Molecular Imaging Center, supported by the Helen Wills Neuroscience Institute. We thank Holly Aaron and Feather Ives for their microscopy training and assistance.

Conflict of interest

The authors report no competing interests.

Figure 1

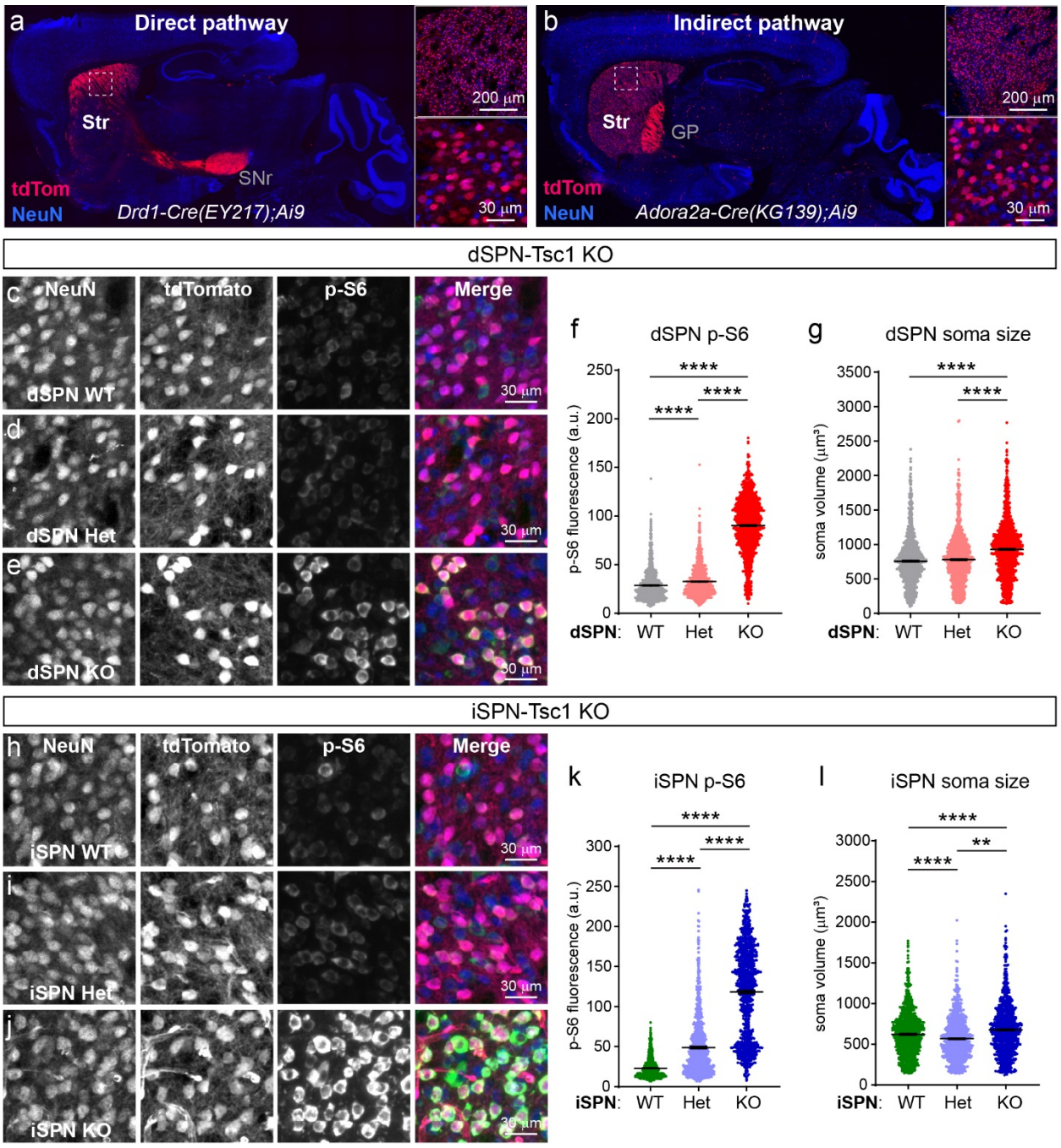
a
Direct pathway
Str
SNr
tdTom
NeuN
Drd1-Cre(EY217);Ai9
200 µm
30 µm
b
Indirect pathway
Str
GP
tdTom
NeuN
Adora2a-Cre(KG139);Ai9
200 µm
30 µm
dSPN-Tsc1 KO
c
NeuN
tdTomato
p-S6
Merge
dSPN WT
d
dSPN Het
e
dSPN KO
30 µm
f
dSPN p-S6
p-S6 fluorescence (a.u.)
****
dSPN: WT Het KO
g
dSPN soma size
soma volume (µm³)
iSPN-Tsc1 KO
h
iSPN WT
i
iSPN Het
j
iSPN KO
k
iSPN p-S6
iSPN: WT Het KO
l
iSPN soma size
**

Figure 1. Developmental loss of *Tsc1* from striatal neurons induces mTORC1 activation and somatic hypertrophy.

(a,b) Images of sagittal brain sections showing the expression pattern of a tdTomato Cre reporter in a *Drd1-Cre;Ai9* mouse (a) and an *Adora2a-Cre;Ai9* mouse (b) with selective expression in the direct and indirect pathways, respectively. Right panels show higher magnification images of the dorsal striatum (boxed region). Str=striatum, SNr=substantia nigra pars reticulata, GP=globus pallidus

(c-e) Confocal images of dorsolateral striatum from a dSPN-Tsc1 WT (c), Tsc1 Het (d), and Tsc1 KO (e) mouse labeled with antibodies against phosphorylated S6 (p-S6, Ser240/244, green in the merged image) and NeuN (blue in the merged image). TdTomato (red in the merged imaged) is expressed in dSPNs.

(f-g) Quantification of dSPN p-S6 fluorescence intensity (f) and soma volume (g) per cell. Horizontal lines indicate the mean +/- SEM. n=1161 neurons from 3 mice per genotype. For panel f, $p<0.0001$, Kruskal-Wallis test; ****, $p<0.0001$ multiple comparisons tests. For panel g, $p<0.0001$, Kruskal-Wallis test; ****, $p<0.0001$; WT vs Het, $p=0.0857$, multiple comparisons tests.

(h-j) Confocal images of dorsolateral striatum from an iSPN-Tsc1 WT (c), Tsc1 Het (d), and Tsc1 KO (e) mouse labeled with antibodies against phosphorylated S6 (p-S6, Ser240/244, green in the merged image) and NeuN (blue in the merged image). TdTomato (red in the merged imaged) is expressed in iSPNs.

(k,l) Quantification of iSPN p-S6 fluorescence intensity (k) and soma volume (l) per cell. Horizontal lines indicate the mean +/- SEM. n=936 neurons from 3 mice for iSPN-WT and 4 mice for iSPN-Het and KO. For panel k, $p<0.0001$, Kruskal-Wallis test; ****, $p<0.0001$ multiple comparisons tests. For panel l, $p<0.0001$, Kruskal-Wallis test; ****, $p<0.0001$, **, $p=0.0020$, multiple comparisons tests.

Figure 2

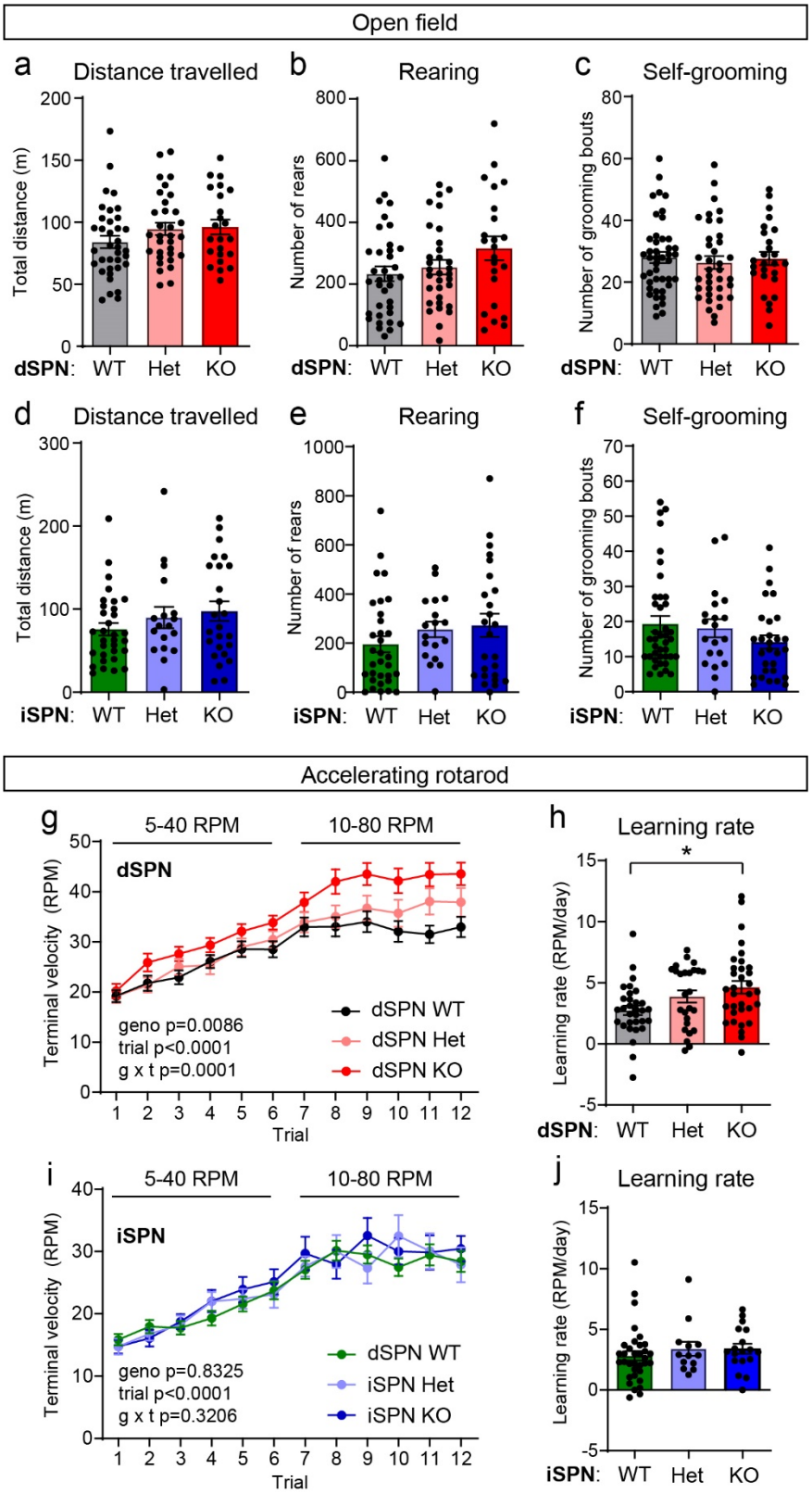
Open field
a
Distance travelled
Total distance (m)
dSPN: WT Het KO
b
Rearing
Number of rears
dSPN: WT Het KO
c
Self-grooming
Number of grooming bouts
dSPN: WT Het KO
d
Distance travelled
Total distance (m)
iSPN: WT Het KO
e
Rearing
Number of rears
iSPN: WT Het KO
f
Self-grooming
Number of grooming bouts
iSPN: WT Het KO
Accelerating rotarod
g
5-40 RPM
10-80 RPM
dSPN
Terminal velocity (RPM)
geno p=0.0086
trial p<0.0001
g x t p=0.0001
dSPN WT
dSPN Het
dSPN KO
Trial
h
Learning rate
Learning rate (RPM/day)
dSPN: WT Het KO
i
5-40 RPM
10-80 RPM
iSPN
Terminal velocity (RPM)
geno p=0.8325
trial p<0.0001
g x t p=0.3206
dSPN WT
iSPN Het
iSPN KO
Trial
j
Learning rate
Learning rate (RPM/day)
iSPN: WT Het KO

Figure 2. Loss of *Tsc1* from dSPNs enhances motor routine learning.

(a-f) Quantification of open field parameters in dSPN- (a-c) and iSPN- (d-f) Tsc1 WT, Het, and KO mice. Distance travelled is the total distance travelled in the open field over 60 minutes. Rearing is the number of rears in 60 minutes. Self-grooming is the number of grooming bouts in the first 20 minutes of the open field test. Bars represent mean +/- SEM. Dots represent individual mice. dSPN-WT n=36, dSPN-Het n=32, dSPN-KO n=23, iSPN-WT n=32, iSPN-Het n=18, iSPN-KO n=25 mice. For panel a, p=0.2006; panel b, p=0.1252 (one-way ANOVA); panel c, p=0.8112 (one-way ANOVA); panel d, p=0.4028; panel e, p=0.2367; panel f, p=0.2497; Kruskal-Wallis tests except where noted.

(g) Accelerating rotarod learning curve in dSPN-Tsc1 WT (n=31 mice), Het (n=26 mice), and KO (n=33 mice). Circles represent mean +/- SEM. Mixed-effects analysis p values are shown. RPM = revolutions per minute.

(h) Rotarod learning rate in dSPN-Tsc1 WT, Het and KO mice calculated as the slope of the line of performance on the first trial to the last trial for each mouse (RPM/day). Bars represent mean +/- SEM. Dots represent individual mice. p=0.0343, Kruskal-Wallis test; *, p=0.0206, multiple comparisons test (dSPN WT vs KO), p=0.2199 (dSPN WT vs Het). n is the same as for panel g.

(i) Accelerating rotarod learning curve in iSPN-Tsc1 WT (n=34 mice), Het (n=13 mice), and KO (n=18 mice). Dots represent mean +/- SEM. Two-way ANOVA p values are shown.

(j) Rotarod learning rate in iSPN-Tsc1 WT, Het and KO mice calculated as the slope of the line of performance on the first trial to the last trial for individual mice (RPM/day). Bars represent mean +/- SEM. Dots represent individual mice. p=0.2761, Kruskal-Wallis test. n is the same as for panel i.

Figure 3

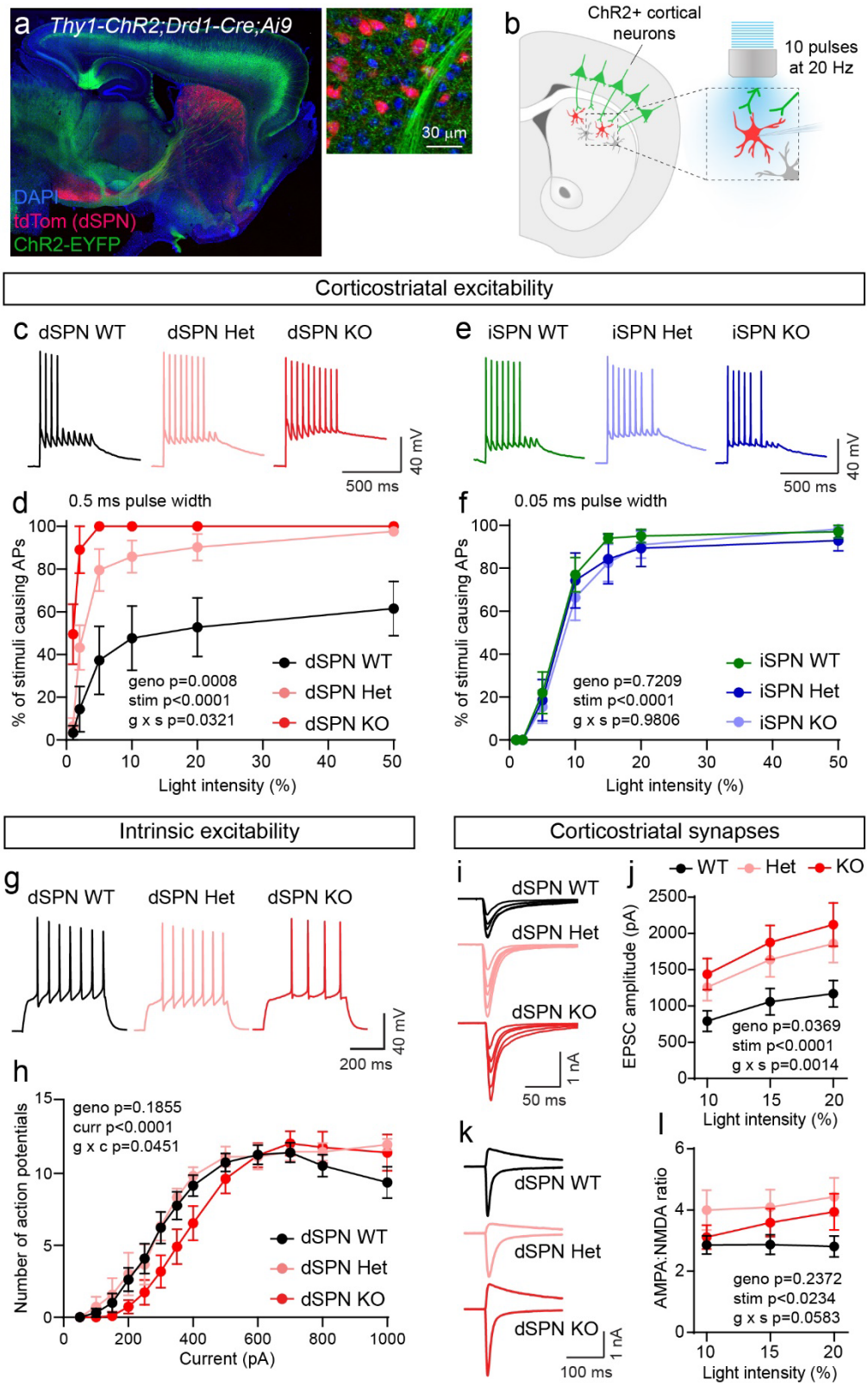
a
Thy1-ChR2;Drd1-Cre;Ai9
DAPI
tdTom (dSPN)
ChR2-EYFP
30 µm
b
ChR2+ cortical neurons
10 pulses at 20 Hz
Corticostriatal excitability
c
dSPN WT
dSPN Het
dSPN KO
40 mV
500 ms
e
iSPN WT
iSPN Het
iSPN KO
40 mV
500 ms
d
0.5 ms pulse width
% of stimuli causing APs
Light intensity (%)
geno p=0.0008
stim p<0.0001
g x s p=0.0321
dSPN WT
dSPN Het
dSPN KO
f
0.05 ms pulse width
% of stimuli causing APs
Light intensity (%)
geno p=0.7209
stim p<0.0001
g x s p=0.9806
iSPN WT
iSPN Het
iSPN KO
Intrinsic excitability
g
dSPN WT
dSPN Het
dSPN KO
40 mV
200 ms
h
Number of action potentials
Current (pA)
geno p=0.1855
curr p<0.0001
g x c p=0.0451
dSPN WT
dSPN Het
dSPN KO
Corticostriatal synapses
i
dSPN WT
dSPN Het
dSPN KO
1 nA
50 ms
j
WT
Het
KO
EPSC amplitude (pA)
Light intensity (%)
geno p=0.0369
stim p<0.0001
g x s p=0.0014
k
dSPN WT
dSPN Het
dSPN KO
1 nA
100 ms
l
AMPA:NMDA ratio
Light intensity (%)
geno p=0.2372
stim p<0.0234
g x s p=0.0583

Figure 3. Tsc1 loss selectively increases cortico-dSPN synaptic drive.

(a) Confocal image of a sagittal brain section from a *Tsc1^{cKO};Thy1-ChR2-EYFP*;*Drd1-Cre;Ai9* mouse. Right image shows cortical terminals expressing ChR2-EYFP in the dorsal striatum.
(b) Schematic of the experiment. Cortical terminals expressing ChR2 were stimulated with 10 pulses of blue light at 20 Hz and responses were recorded in identified dSPNs in dorsolateral striatum. For dSPNs, the pulse width was 0.5 ms and for iSPNs the pulse width was 0.05 ms.
(c,d) Example traces at 10% light intensity (c) and quantification as an input-output curve (mean +/- SEM) of action potentials (APs) evoked in dSPNs by cortical terminal stimulation (d) (*Tsc1^{cKO};Thy1-ChR2-EYFP*;*Drd1-Cre;Ai9* mice). dSPN-Tsc1 WT n=5, dSPN Het n=7, dSPN KO n=5 neurons. Two-way ANOVA p values are shown.
(e,f) Example traces at 10% light intensity (e) and quantification as an input-output curve (mean +/- SEM) of APs evoked in iSPNs by cortical terminal stimulation (f) (*Tsc1^{cKO};Thy1-ChR2-EYFP*;*Adora2a-Cre;Ai9* mice). iSPN-Tsc1 WT n=10, dSPN Het n=11, dSPN KO n=7 neurons. Two-way ANOVA p values are shown.
(g,h) Example traces from a 350 pA current step (g) and quantification (h) of the number of APs induced by depolarizing current steps in dSPN-Tsc1 WT, Het and KO neurons (*Tsc1^{cKO};Drd1-Cre;Ai9* mice). Circles represent mean +/- SEM. dSPN WT n=13, dSPN Het n=6, dSPN KO n=11 neurons. Mixed-effects analysis p values are shown.
(i) Example traces show EPSCs induced by corticostriatal stimulation at different light intensities (5-20%) in dSPN-Tsc1 WT, Het and KO neurons (*Tsc1^{cKO};Thy1-ChR2-EYFP*;*Drd1-Cre;Ai9* mice).
(j) Quantification of corticostriatal EPSC amplitude in dSPN WT, Het and KO neurons induced by different light intensities (0.5 ms pulse width). Circles represent mean +/- SEM. dSPN-Tsc1 WT n=18, dSPN Het n=7, dSPN KO n=25 neurons. Mixed-effects analysis p values are shown.
(k) Example traces show pairs of EPSCs recorded at +40 mV (top traces) and -80 mV (bottom traces) from dSPN-Tsc1 WT, Het and KO neurons (*Tsc1^{cKO};Thy1-ChR2-EYFP*;*Drd1-Cre;Ai9* mice).
(l) Quantification of AMPA:NMDA ratio per cell in dSPN WT, Het and KO neurons across different intensities of corticostriatal stimulation. Circles represent mean +/- SEM. dSPN-Tsc1 WT n=9, dSPN Het n=7, dSPN KO n=14 neurons. Two-way ANOVA p values are shown.

Figure 4

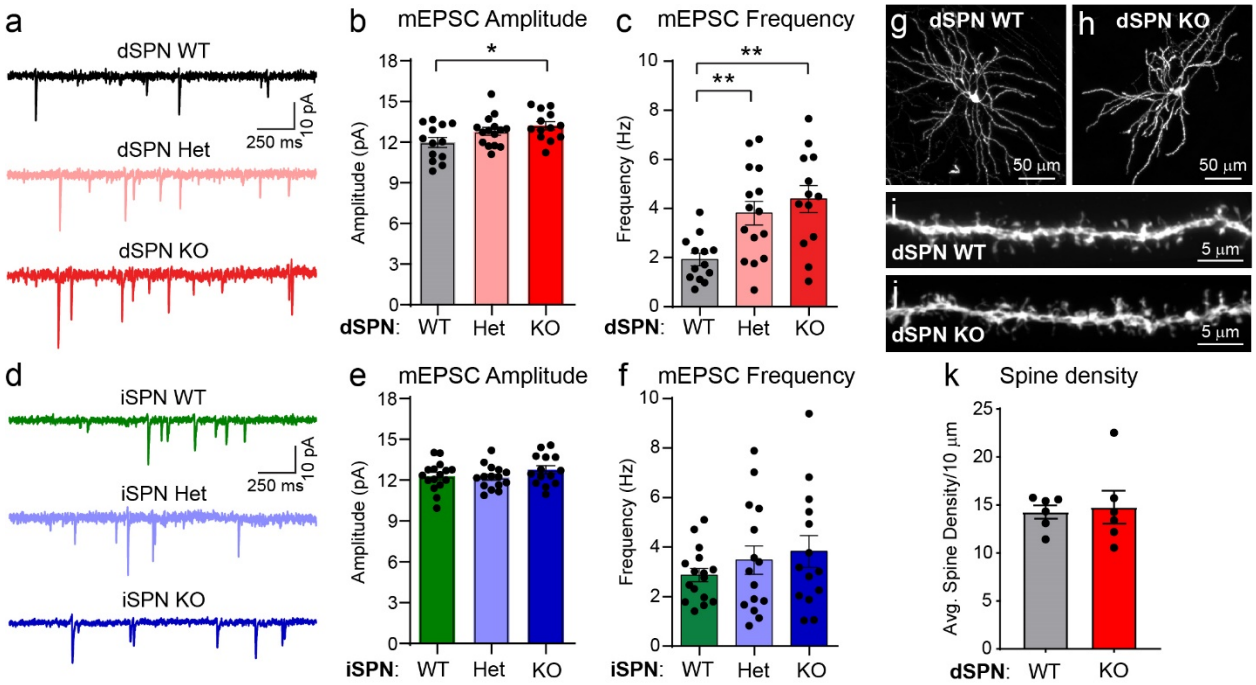
a
dSPN WT
dSPN Het
dSPN KO
10 pA
250 ms
b mEPSC Amplitude
Amplitude (pA)
dSPN: WT Het KO
c mEPSC Frequency
Frequency (Hz)
dSPN: WT Het KO
g dSPN WT
h dSPN KO
50 µm
i dSPN WT
j dSPN KO
5 µm
d
iSPN WT
iSPN Het
iSPN KO
10 pA
250 ms
e mEPSC Amplitude
Amplitude (pA)
iSPN: WT Het KO
f mEPSC Frequency
Frequency (Hz)
iSPN: WT Het KO
k Spine density
Avg. Spine Density/10 µm
dSPN: WT KO

Figure 4. Loss of Tsc1 increases excitatory synaptic transmission onto dSPNs.

(a) Example traces of mEPSCs recorded from dSPN-Tsc1 WT, Het and KO neurons.

(b,c) Mean +/- SEM mEPSC amplitude (b) and frequency (c) recorded from dSPN-Tsc1 WT, Het and KO neurons. Dots represent individual neurons. For panel b, p=0.0337, one-way ANOVA; *, p=0.0324 (dSPN WT vs KO), p=0.1473 (dSPN WT vs Het), p=0.3479 (dSPN Het vs KO), Holm-Sidak's multiple comparisons tests. For panel c, p=0.0014, one-way ANOVA; **, p=0.0099 (dSPN WT vs Het), **, p=0.0017 (dSPN WT vs KO), p=0.3668 (dSPN Het vs KO), Holm-Sidak's multiple comparisons tests. For both b and c, dSPN WT n=13, dSPN Het n=15, dSPN KO n=13 neurons.

(d) Example traces of mEPSCs recorded from iSPN-Tsc1 WT, Het and KO neurons.

(e,f) Mean +/- SEM mEPSC amplitude (e) and frequency (f) recorded from iSPN-Tsc1 WT, Het and KO neurons. Dots represent individual neurons. For panel e, p=0.2942, one-way ANOVA. For panel f, p=0.4083, one-way ANOVA. For both e and f, iSPN WT n=16, iSPN Het n=15, iSPN KO n=14 neurons.

(g-h) Confocal images of individual Tsc1 WT (g) and KO (h) dSPNs labeled in *Tsc1;Drd1-Cre* mice using an AAV expressing Cre-dependent tdTomato.

(i-j) Representative images of dendritic spines from a Tsc1 WT (i) and KO (j) dSPN.

(k) Quantification of dendritic spine density in Tsc1 WT and KO dSPNs. Data are represented as mean +/- SEM spine density per 10 μm of dendrite. Dots display the average spine density for individual neurons. dSPN WT n=6 neurons (12 dendrites) from 3 mice, dSPN KO n=6 neurons (13 dendrites) from 3 mice. p=0.8182, Mann-Whitney test.

Figure 5

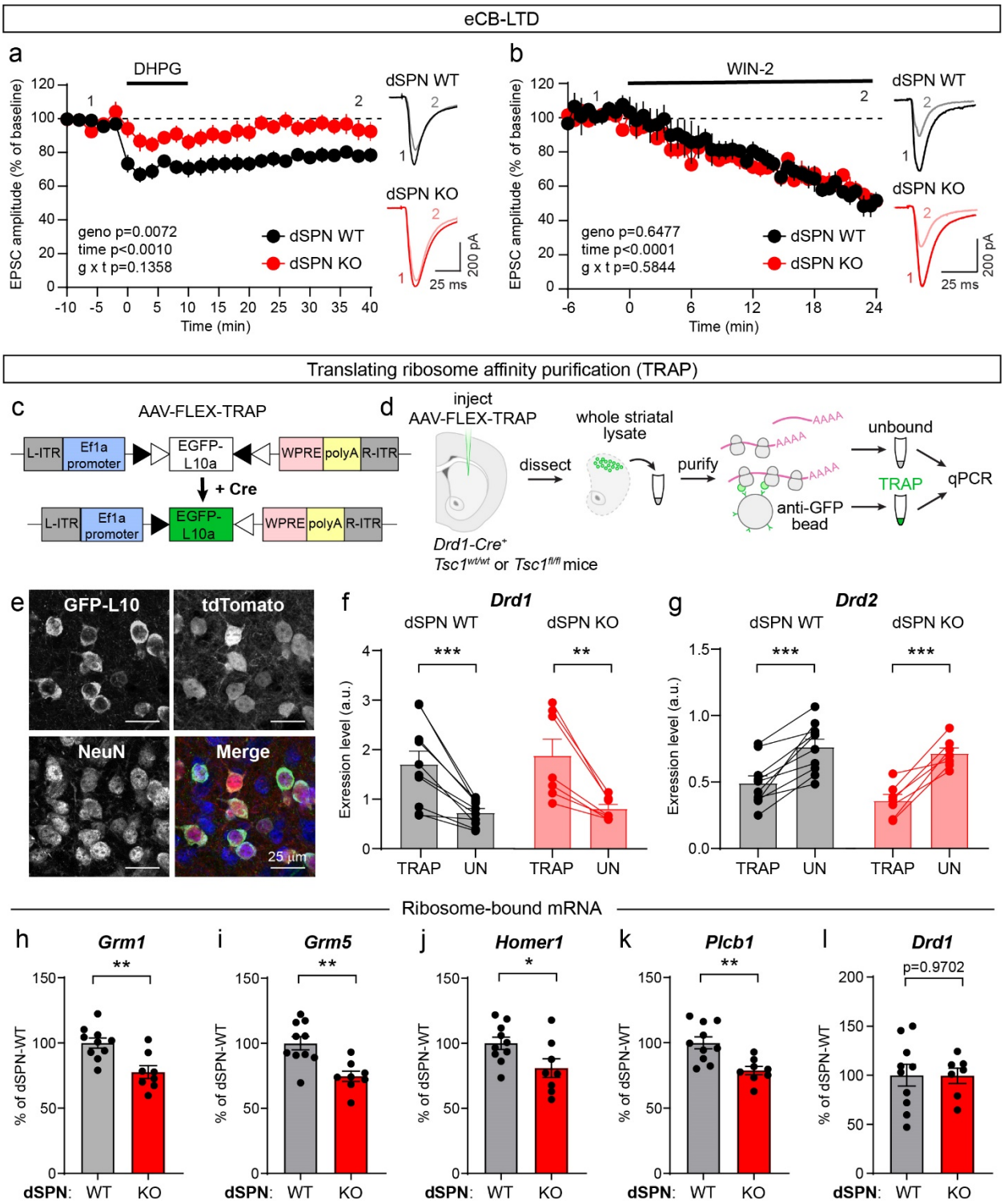
eCB-LTD
a
DHPG
EPSC amplitude (% of baseline)
Time (min)
geno p=0.0072
time p<0.0010
g x t p=0.1358
dSPN WT
dSPN KO
200 pA
25 ms
b
WIN-2
geno p=0.6477
time p<0.0001
g x t p=0.5844
Translating ribosome affinity purification (TRAP)
c
AAV-FLEX-TRAP
L-ITR
Ef1a promoter
EGFP-L10a
WPRE
polyA
R-ITR
+ Cre
d
inject AAV-FLEX-TRAP
dissect
whole striatal lysate
purify
unbound
TRAP
qPCR
anti-GFP bead
Drd1-Cre+
Tsc1wt/wt or Tsc1fl/fl mice
e
GFP-L10
tdTomato
NeuN
Merge
25 µm
f
Drd1
dSPN WT
dSPN KO
Exression level (a.u.)
TRAP
UN
g
Drd2
Ribosome-bound mRNA
h
Grm1
% of dSPN-WT
dSPN: WT KO
i
Grm5
j
Homer1
k
Plcb1
l
Drd1
p=0.9702

Figure 5. dSPN-Tsc1 KO neurons have impaired eCB-LTD.

(a) Corticostriatal terminals in the dorsolateral striatum were stimulated with blue light (30s ISI) to evoke EPSCs in dSPN-Tsc1 WT and KO neurons (*Tsc1^{cKO};Thy1-ChR2-EYFP*;*Drd1-Cre;Ai9* mice). Following a 10 minute baseline period, DHPG (100 μM) was washed on for 10 minutes. Data are presented as mean +/- SEM percent of baseline. P values for mixed-effects analysis are shown. dSPN WT n=7, dSPN KO n=5 neurons. Example traces on the right show average EPSCs from the baseline period ("1") and 35-40 minutes after DHPG application ("2").

(b) Corticostriatal terminals were stimulated with blue light (30s ISI) to evoke EPSCs in dSPN-Tsc1 WT and KO neurons (*Tsc1^{cKO};Thy1-ChR2-EYFP*;*Drd1-Cre;Ai9* mice). WIN2 (2 μM) was applied at time 0 to activate CB1 receptors. Data are presented as mean +/- SEM percent of baseline. P values for mixed-effects analysis are shown. dSPN WT n=5, dSPN KO n=4 neurons. Example traces on the right show the average EPSC from the last 5 minutes of the baseline period ("1") and 19-24 minutes after WIN-2 application ("2").

(c) Schematic of the design of AAV-FLEX-TRAP, which allows Cre-dependent expression of a GFP-tagged ribosomal subunit (EGFP-L10a).

(d) Schematic of the workflow for the Translational Ribosome Affinity Purification (TRAP) experiment.

(e) Images of EGFP-L10a expression from an AAV5-hSyn-DIO-EGFP-L10a-WPRE-hGH in the dorsolateral striatum of a *Tsc1^{cKO};Thy1-ChR2;Drd1-Cre;Ai9* mouse showing expression in tdTomato+ dSPNs.

(f) Quantification of relative *Drd1* (f) and *Drd2* (g) mRNA levels in TRAP samples (ribosome bound mRNA isolated from dSPNs) versus the unbound (all striatal tissue) from the same mouse measured by qPCR. Bars represent mean +/- SEM. Dots represent individual samples, taken from one mouse. For panel f, ***, p=0.0009 (dSPN WT); **, p=0.0053 (dSPN KO), paired t-tests. For panel g, ***, p=0.0003 (dSPN WT); ***, p=0.0007 (dSPN KO), paired t-tests.
For panels f and g, dSPN WT n=10 and dSPN KO n=7 mice.

(h-l) Quantification of *Grm1* (h), *Grm5* (i), *Homer1* (j), *Plcb1* (k), and *Drd1* (l) mRNA levels in TRAP samples (ribosome bound mRNA isolated from dSPNs) relative to *Actb* from dSPN-Tsc1 WT and KO mice measured by qPCR. Bars represent mean +/- SEM and dots represent individual mice. For panel h, **, p=0.0022; panel i, **, p=0.0018; panel j, *, p=0.0346; panel k, **, p=0.0025; panel l, p=0.9702; unpaired t-tests. For all panels, dSPN WT n=10 and dSPN KO n=8 mice (except for *Drd1* dSPN KO, n=7 mice).

References

1. Association., A.P., *Diagnostic and statistical manual of mental disorders : DSM-5. 5th edn.* 2013.
2. De Rubeis, S., et al., *Synaptic, transcriptional and chromatin genes disrupted in autism.* Nature, 2014. **515**(7526): p. 209-15.
3. An, J.Y., et al., *Genome-wide de novo risk score implicates promoter variation in autism spectrum disorder.* Science, 2018. **362**(6420).
4. Cross-Disorder Group of the Psychiatric Genomics, C., et al., *Genetic relationship between five psychiatric disorders estimated from genome-wide SNPs.* Nat Genet, 2013. **45**(9): p. 984-94.
5. SFARI. *SFARI Gene*. 2019 [cited 2019 July 15]; Available from: https://gene.sfari.org/.
6. Curatolo, P., R. Moavero, and P.J. de Vries, *Neurological and neuropsychiatric aspects of tuberous sclerosis complex.* The Lancet Neurology, 2015. **14**(7): p. 733-745.
7. Saxton, R.A. and D.M. Sabatini, *mTOR Signaling in Growth, Metabolism, and Disease.* Cell, 2017. **168**(6): p. 960-976.
8. de Vries, P.J., *Targeted Treatments for Cognitive and Neurodevelopmental Disorders in Tuberous Sclerosis Complex.* Neurotherapeutics, 2010. **7**: p. 275-282.
9. Tang, G., et al., *Loss of mTOR-Dependent Macroautophagy Causes Autistic-like Synaptic Pruning Deficits.* Neuron, 2014. **83**(5): p. 1131-43.
10. Kelleher, R.J., 3rd and M.F. Bear, *The autistic neuron: troubled translation?* Cell, 2008. **135**(3): p. 401-6.
11. Fuccillo, M.V., *Striatal Circuits as a Common Node for Autism Pathophysiology.* Front Neurosci, 2016. **10**: p. 27.
12. Turner, K.C., et al., *Atypically diffuse functional connectivity between caudate nuclei and cerebral cortex in autism.* Behav Brain Funct, 2006. **2**: p. 34.
13. Qiu, A., et al., *Basal ganglia shapes predict social, communication, and motor dysfunctions in boys with autism spectrum disorder.* J Am Acad Child Adolesc Psychiatry, 2010. **49**(6): p. 539-51, 551 e1-4.
14. Di Martino, A., et al., *Aberrant striatal functional connectivity in children with autism.* Biol Psychiatry, 2011. **69**(9): p. 847-56.
15. Asano, E., D.C. Chugani, O. Muzik, M. Behen, J. Janisse, R. Rothermel, T.J. Mangner, P.K. Chakraborty, H.T. Chugani, *Autism in tuberous sclerosis complex is related to both cortical and subcortical dysfunction.* Neurology, 2001. **57**: p. 1269-1277.
16. Rothwell, P.E., et al., *Autism-associated neuroligin-3 mutations commonly impair striatal circuits to boost repetitive behaviors.* Cell, 2014. **158**(1): p. 198-212.
17. Platt, R.J., et al., *Chd8 Mutation Leads to Autistic-like Behaviors and Impaired Striatal Circuits.* Cell Rep, 2017. **19**(2): p. 335-350.
18. Penagarikano, O., et al., *Absence of CNTNAP2 leads to epilepsy, neuronal migration abnormalities, and core autism-related deficits.* Cell, 2011. **147**(1): p. 235-46.
19. Nakatani, J., et al., *Abnormal behavior in a chromosome-engineered mouse model for human 15q11-13 duplication seen in autism.* Cell, 2009. **137**(7): p. 1235-46.
20. Peixoto, R.T., et al., *Early hyperactivity and precocious maturation of corticostriatal circuits in Shank3B(-/-) mice.* Nat Neurosci, 2016. **19**(5): p. 716-24.
21. Jaramillo, T.C., et al., *Altered Striatal Synaptic Function and Abnormal Behaviour in Shank3 Exon4-9 Deletion Mouse Model of Autism.* Autism Res, 2016. **9**(3): p. 350-75.
22. Wang, X., et al., *Altered mGluR5-Homer scaffolds and corticostriatal connectivity in a Shank3 complete knockout model of autism.* Nat Commun, 2016. **7**: p. 11459.
23. Benthall, K.N., S.L. Ong, and H.S. Bateup, *Corticostriatal Transmission Is Selectively Enhanced in Striatonigral Neurons with Postnatal Loss of Tsc1.* Cell Rep, 2018. **23**(11): p. 3197-3208.

24. Graybiel, A.M., *The basal ganglia: learning new tricks and loving it.* Curr Opin Neurobiol, 2005. **15**(6): p. 638-44.
25. Gertler, T.S., C.S. Chan, and D.J. Surmeier, *Dichotomous anatomical properties of adult striatal medium spiny neurons.* J Neurosci, 2008. **28**(43): p. 10814-24.
26. Heiman, M., et al., *A translational profiling approach for the molecular characterization of CNS cell types.* Cell, 2008. **135**(4): p. 738-48.
27. Gerfen, C.R. and D.J. Surmeier, *Modulation of striatal projection systems by dopamine.* Annu Rev Neurosci, 2011. **34**: p. 441-66.
28. Kravitz, A.V., et al., *Regulation of parkinsonian motor behaviours by optogenetic control of basal ganglia circuitry.* Nature, 2010. **466**(7306): p. 622-6.
29. Tai, L.H., et al., *Transient stimulation of distinct subpopulations of striatal neurons mimics changes in action value.* Nat Neurosci, 2012. **15**(9): p. 1281-9.
30. Kreitzer, A.C., *Physiology and pharmacology of striatal neurons.* Annu Rev Neurosci, 2009. **32**: p. 127-47.
31. Bateup, H.S., et al., *Distinct subclasses of medium spiny neurons differentially regulate striatal motor behaviors.* Proc Natl Acad Sci U S A, 2010. **107**(33): p. 14845-50.
32. Graybiel, A.M. and S.T. Grafton, *The striatum: where skills and habits meet.* Cold Spring Harb Perspect Biol, 2015. **7**(8): p. a021691.
33. Kwiatkowski, D.J., *A mouse model of TSC1 reveals sex-dependent lethality from liver hemangiomas, and up-regulation of p70S6 kinase activity in Tsc1 null cells.* Human Molecular Genetics, 2002. **11**(5): p. 525-534.
34. Gong, S., et al., *Targeting Cre recombinase to specific neuron populations with bacterial artificial chromosome constructs.* J Neurosci, 2007. **27**(37): p. 9817-23.
35. Madisen, L., et al., *A robust and high-throughput Cre reporting and characterization system for the whole mouse brain.* Nat Neurosci, 2010. **13**(1): p. 133-40.
36. Arenkiel, B.R., et al., *In vivo light-induced activation of neural circuitry in transgenic mice expressing channelrhodopsin-2.* Neuron, 2007. **54**(2): p. 205-18.
37. Onda, H., Andreas Lueck, Peter W. Marks, Henry B. Warren, David J. Kwiatkowski, *Tsc2+/- mice develop tumors in multiple sites that express gelsolin and are influenced by genetic background.* The Journal of Clinical Investigation, 1999. **104**(6).
38. Heiman, M., et al., *Cell type-specific mRNA purification by translating ribosome affinity purification (TRAP).* Nat Protoc, 2014. **9**(6): p. 1282-91.
39. Lim, J.S., et al., *Somatic Mutations in TSC1 and TSC2 Cause Focal Cortical Dysplasia.* Am J Hum Genet, 2017. **100**(3): p. 454-472.
40. Yin, H.H., et al., *Dynamic reorganization of striatal circuits during the acquisition and consolidation of a skill.* Nat Neurosci, 2009. **12**(3): p. 333-41.
41. Crino, P.B., *Evolving neurobiology of tuberous sclerosis complex.* Acta Neuropathol, 2013. **125**(3): p. 317-32.
42. Curatolo, P., R. Bombardieri, and S. Jozwiak, *Tuberous sclerosis.* The Lancet, 2008. **372**(9639): p. 657-668.
43. de Vries, P.J. and C.J. Howe, *The tuberous sclerosis complex proteins--a GRIPP on cognition and neurodevelopment.* Trends Mol Med, 2007. **13**(8): p. 319-26.
44. Bateup, H.S., et al., *Excitatory/Inhibitory synaptic imbalance leads to hippocampal hyperexcitability in mouse models of tuberous sclerosis.* Neuron, 2013. **78**(3): p. 510-22.
45. Bateup, H.S., et al., *Loss of Tsc1 in vivo impairs hippocampal mGluR-LTD and increases excitatory synaptic function.* J Neurosci, 2011. **31**(24): p. 8862-9.
46. Normand, E.A., et al., *Temporal and mosaic Tsc1 deletion in the developing thalamus disrupts thalamocortical circuitry, neural function, and behavior.* Neuron, 2013. **78**(5): p. 895-909.
47. Tavazoie, S.F., et al., *Regulation of neuronal morphology and function by the tumor suppressors Tsc1 and Tsc2.* Nat Neurosci, 2005. **8**(12): p. 1727-34.

48. Tsai, P.T., et al., *Autistic-like behaviour and cerebellar dysfunction in Purkinje cell Tsc1 mutant mice.* Nature, 2012. **488**(7413): p. 647-51.
49. Weston, M.C., H. Chen, and J.W. Swann, *Loss of mTOR repressors Tsc1 or Pten has divergent effects on excitatory and inhibitory synaptic transmission in single hippocampal neuron cultures.* Front Mol Neurosci, 2014. **7**: p. 1.
50. Zeng, L.H., et al., *Abnormal glutamate homeostasis and impaired synaptic plasticity and learning in a mouse model of tuberous sclerosis complex.* Neurobiol Dis, 2007. **28**(2): p. 184-96.
51. Zhao, J.P. and A. Yoshii, *Hyperexcitability of the local cortical circuit in mouse models of tuberous sclerosis complex.* Mol Brain, 2019. **12**(1): p. 6.
52. Kosillo, P., et al., *Tsc1-mTORC1 signaling controls striatal dopamine release and cognitive flexibility.* Nat Commun, 2019. **10**(1): p. 5426.
53. Yang, S.B., et al., *Rapamycin ameliorates age-dependent obesity associated with increased mTOR signaling in hypothalamic POMC neurons.* Neuron, 2012. **75**(3): p. 425-36.
54. Malik, R., et al., *Tsc1 represses parvalbumin expression and fast-spiking properties in somatostatin lineage cortical interneurons.* Nat Commun, 2019. **10**(1): p. 4994.
55. Ehninger, D., et al., *Reversal of learning deficits in a Tsc2(+/-) mouse model of tuberous sclerosis.* Nat Med, 2008. **14**(8): p. 843-8.
56. Kuo, H.Y. and F.C. Liu, *Synaptic Wiring of Corticostriatal Circuits in Basal Ganglia: Insights into the Pathogenesis of Neuropsychiatric Disorders.* eNeuro, 2019. **6**(3).
57. Doig, N.M., J. Moss, and J.P. Bolam, *Cortical and thalamic innervation of direct and indirect pathway medium-sized spiny neurons in mouse striatum.* J Neurosci, 2010. **30**(44): p. 14610-8.
58. Kreitzer, A.C. and R.C. Malenka, *Striatal plasticity and basal ganglia circuit function.* Neuron, 2008. **60**(4): p. 543-54.
59. Lovinger, D.M., *Neurotransmitter roles in synaptic modulation, plasticity and learning in the dorsal striatum.* Neuropharmacology, 2010. **58**(7): p. 951-61.
60. Kreitzer, A.C. and R.C. Malenka, *Endocannabinoid-mediated rescue of striatal LTD and motor deficits in Parkinson's disease models.* Nature, 2007. **445**(7128): p. 643-7.
61. Wu, Y.W., et al., *Input- and cell-type-specific endocannabinoid-dependent LTD in the striatum.* Cell Rep, 2015. **10**(1): p. 75-87.
62. Chevere-Torres, I., et al., *Metabotropic glutamate receptor-dependent long-term depression is impaired due to elevated ERK signaling in the DeltaRG mouse model of tuberous sclerosis complex.* Neurobiol Dis, 2012. **45**(3): p. 1101-10.
63. Auerbach, B.D., E.K. Osterweil, and M.F. Bear, *Mutations causing syndromic autism define an axis of synaptic pathophysiology.* Nature, 2011. **480**(7375): p. 63-8.
64. Potter, W.B., et al., *Reduced juvenile long-term depression in tuberous sclerosis complex is mitigated in adults by compensatory recruitment of mGluR5 and Erk signaling.* PLoS Biol, 2013. **11**(8): p. e1001627.
65. Shonesy, B.C., et al., *Role of Striatal Direct Pathway 2-Arachidonoylglycerol Signaling in Sociability and Repetitive Behavior.* Biol Psychiatry, 2018. **84**(4): p. 304-315.
66. Ohno-Shosaku, T. and M. Kano, *Endocannabinoid-mediated retrograde modulation of synaptic transmission.* Curr Opin Neurobiol, 2014. **29**: p. 1-8.
67. Gobet, C. and F. Naef, *Ribosome profiling and dynamic regulation of translation in mammals.* Curr Opin Genet Dev, 2017. **43**: p. 120-127.
68. Ingolia, N.T., L.F. Lareau, and J.S. Weissman, *Ribosome profiling of mouse embryonic stem cells reveals the complexity and dynamics of mammalian proteomes.* Cell, 2011. **147**(4): p. 789-802.
69. Kalueff, A.V., et al., *Neurobiology of rodent self-grooming and its value for translational neuroscience.* Nat Rev Neurosci, 2016. **17**(1): p. 45-59.

70. Bey, A.L., Wang, X., Yan, H., Kim, N., Passman, R. L., Yang, Y., … Jiang, Y., *Brain region-specific disruption of Shank3 in mice.* Translational Psychiatry, 2018. **8**(1).
71. Bergeron, Y., et al., *mTOR signaling contributes to motor skill learning in mice.* Front Mol Neurosci, 2014. **7**: p. 26.
72. Kwon, C.H., et al., *Pten regulates neuronal arborization and social interaction in mice.* Neuron, 2006. **50**(3): p. 377-88.
73. Portmann, T., et al., *Behavioral abnormalities and circuit defects in the basal ganglia of a mouse model of 16p11.2 deletion syndrome.* Cell Rep, 2014. **7**(4): p. 1077-1092.
74. Sato, A., et al., *Rapamycin reverses impaired social interaction in mouse models of tuberous sclerosis complex.* Nat Commun, 2012. **3**: p. 1292.
75. Piochon, C., M. Kano, and C. Hansel, *LTD-like molecular pathways in developmental synaptic pruning.* Nat Neurosci, 2016. **19**(10): p. 1299-310.
76. Lieberman, O.J., et al., *Dopamine Triggers the Maturation of Striatal Spiny Projection Neuron Excitability during a Critical Period.* Neuron, 2018. **99**(3): p. 540-554 e4.